Lab on a Chip

Micro- & nano- fluidic research for chemistry, physics, biology, & bioengineering

www.rsc.org/loc

Volume 11 | Number 11 | 7 June 2011 | Pages 1841–1980

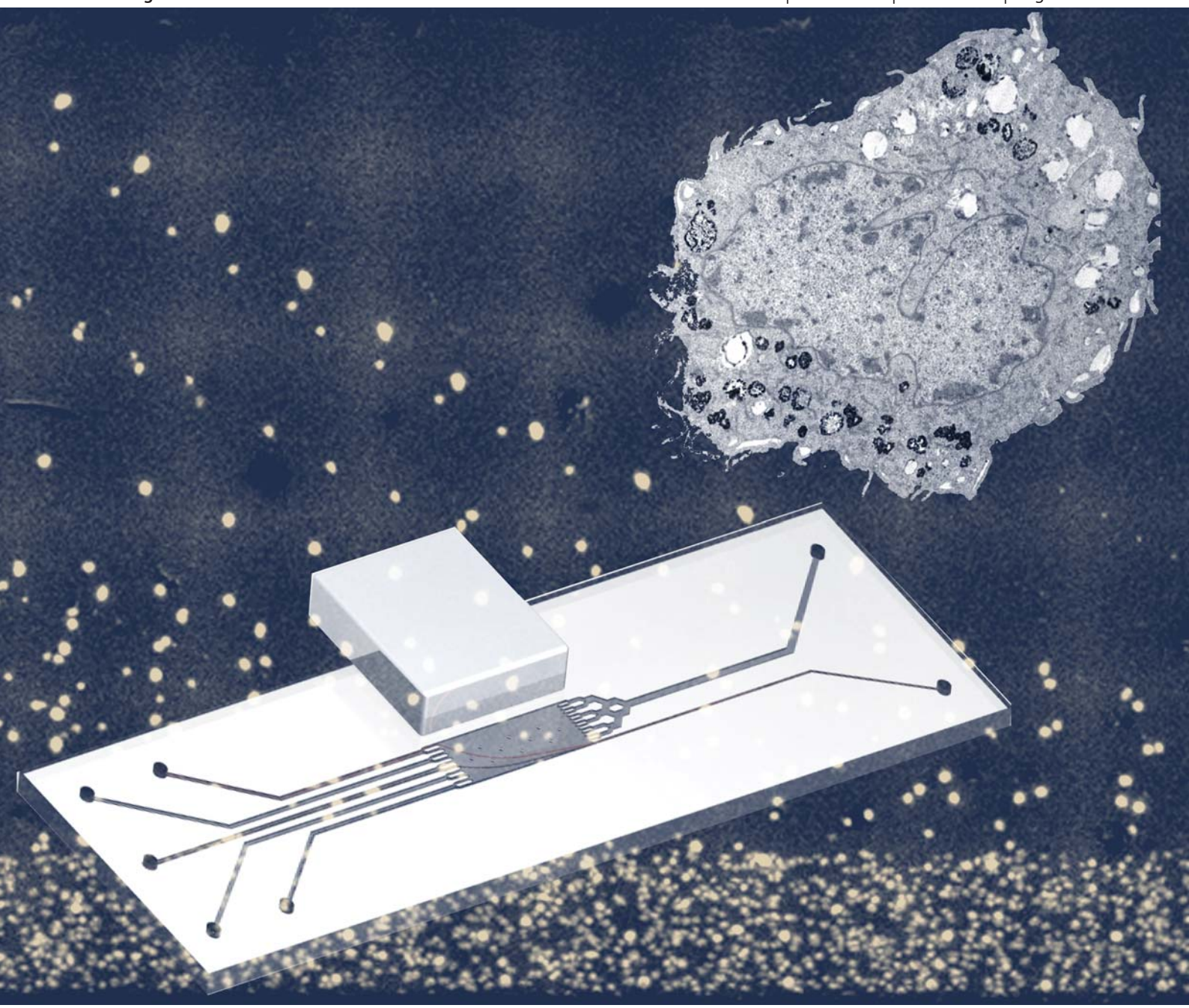

ISSN 1473-0197

RSC Publishing

PAPER

Pamme and Wilhelm *et al.*

Cell sorting by endocytotic capacity in a microfluidic magnetophoresis device

Lab on a Chip

Dynamic Article Links

Cite this: *Lab Chip*, 2011, **11**, 1902

www.rsc.org/loc

PAPER

Cell sorting by endocytotic capacity in a microfluidic magnetophoresis device

Damien Robert,[a] Nicole Pamme,*[b] Hélène Conjeaud,[a] Florence Gazeau,[a] Alexander Iles[b] and Claire Wilhelm*[a]

Received 3rd December 2010, Accepted 25th March 2011
DOI: 10.1039/c0lc00656d

Magnetically labelled cells are finding a wealth of applications for *in vitro* analysis as well as *in vivo* treatments. Sorting of cells into subpopulations based on their magnetite loading is an important step in such procedures. Here, we study the sorting of monocytes and macrophages which internalise nanoparticles to different extents based on their endocytotic capacity. Macrophages featured a high endocytotic activity and were found to internalise between 4 and 60 pg of iron per cell. They were successfully sorted into five subpopulations of narrow iron loading distributions *via* on-chip free-flow magnetophoresis, thus demonstrating the potential of sorting of relatively similarly loaded cells. Monocytes featured a low endocytotic capacity and took on 1 to 4 pg of iron per cell. Mixtures of monocytes and macrophages were successfully sorted within the free-flow magnetophoresis chip and good purity (>88%), efficacy (>60%) and throughput (from 10 to 100 cells s^{-1}) could be achieved. The introduced method constitutes a viable tool for studies of endocytotic capacity and sorting/selection of cells based on this functionality.

Introduction

Cells labelled with magnetic nanoparticles are an important tool for *in vitro* diagnostics as well as cell based therapies.[1,2] Typically, iron oxide particles with diameters of 5 to 10 nm are employed for such applications. Due to their versatility, they have been considered as nanometric multifunctional agents.[3,4] Example applications include contrast enhancement of cells for Magnetic Resonance Imaging[5] and hyperthermia, in which the nanoparticles act as heating mediators for cancer therapy.[6–8] Magnetic labelling of cells is also studied for drug delivery,[9,10] magnetofection,[11–13] intracellular cell mechanics,[14,15] cell patterning, tissue engineering[16–19] and bioseparation.[2,20] Magnetic particles can bind to the cell surface by molecular recognition between the cell's surface markers and suitable antigens on the particle surface[21–24] or by endocytotic nanoparticle uptake.[25–27]

The isolation, separation and sorting of magnetically labelled cells has therefore attracted significant attention. Most methods are based on isolating magnetically labelled cells from bulk solutions, for example, magnetically activated cell sorting (MACS) methods[21] and immunomagnetic cell capture.[28,29]

Some researchers have made use of the spatial and temporal control offered by microfluidic devices for the handling and trapping of magnetic cells. Toner's group employed antibody-conjugated magnetic nanoparticles to bind to HIV cells which were trapped in a magnetic bed for subsequent lysis and downstream analysis.[30] Other reports involve the specific binding of magnetic microbeads to CD3 T cells[31] or CD3 + T-lymphocytes,[32] which were captured on chip from cell mixtures. Red blood cells, which are naturally magnetic in their deoxygenated state, have also been trapped and isolated from whole blood.[33]

The methods listed above can differentiate only between magnetic and non-magnetic cells. There is however a need for efficient sorting of cells based on nanoparticle uptake. Continuous flow methods[34] such as free-flow magnetophoresis can be employed to deflect microparticles[35,36] or magnetically labelled cells based on their extent of magnetisation.[37] Cells can be injected continuously into the device, thus enabling high throughput and combination with downstream processes. We have previously reported on the magnetic deflection of HeLa tumour cells, based on their magnetite loading, in a free-flow magnetophoresis device.[37] Chalmers' and Zborowski's groups have developed dipole and quadrupole magnetic cell sorters for the sorting of cell populations based on surface markers such as CD45 and CD34.[38,39] A report by Adams *et al.*[24] also dealt with the sorting of target cell populations based on surface marker expression. They embedded magnetisable strips into their separation chamber and guided cells into one of the three outlets. These methods involved specific binding of functionalised nanoparticles to surface markers.

We were interested in demonstrating that natural endocytosis of magnetic nanoparticles could be used as the driving process for differential cell sorting in continuous flow microfluidic devices. The monocyte–macrophage cell system is an ideal candidate for such a study. It consists of macrophages and their precursor cells, monocytes, both derived from hematopoietic stem cells. After differentiation, monocytes enter the circulation

[a]*Laboratoire Matière et Systèmes Complexes (MSC), UMR 7057 CNRS et Université Paris Diderot, Paris, France. E-mail: claire.wilhelm@univ-paris-diderot.fr*
[b]*The University of Hull, Department of Chemistry, Cottingham Road, Hull, HU6 7RX, UK. E-mail: n.pamme@hull.ac.uk*

and migrate into various tissues where they differentiate into macrophages. Macrophages then play a central role in several inflammatory diseases, including sclerosis, ischemic stroke lesions, transplanted graft rejection and bacterial infections.[40] Monocyte recruitment into infection sites or within hypoxic regions of tumors may also be exploited for nanoparticle based therapeutic delivery.[41,42] Furthermore, macrophages were found to exhibit important endocytotic capabilities, especially in comparison to their homologous undifferentiated monocytes.[43]

While some reports exist on the continuous flow sorting of cells based on surface marker expression, microfluidic tools for the continuous flow separation and sorting of cells based on endocytotic capacity have not yet been investigated. Here, we report on the sorting of macrophages and monocytes based on endocytotic capacity in a free-flow magnetophoresis chip with five separate outlets.

Materials and methods

Cell culture

THP1 monocytes were cultured in RPMI 1640 medium containing 10% fetal bovine serum supplemented with 2 mM L-glutamine and 100 U mL^{-1} penicillin–streptomycin at 37 °C in 5% CO_2. Their mean diameter was 13.5 ± 1.9 μm. After treatment with phorbol ester (PMA, 50 ng mL^{-1}, Sigma-Aldrich) for 6 days, THP1 monocytes were fully differentiated into macrophages. These differentiated macrophages were larger in diameter, measuring 18.9 ± 4.4 μm.

Magnetic cell labelling

Magnetic nanoparticles with 8.7 nm diameter were synthesised *via* alkaline co-precipitation of iron(III) and iron(II) salts.[44] The particles featured a core of maghemite (γFe_2O_3) and negative surface charges originating from carboxylate functional groups, which ensured stability in aqueous suspensions. The loading of nanoparticles within a cell can be expressed in pg of iron per cell, where 1 pg corresponds to 8×10^5 nanoparticles.

These nanoparticles have been shown to spontaneously interact with the cell plasma membrane and to be internalised following the endocytotic pathway. It has also been demonstrated that the uptake of these magnetic nanoparticles is non-toxic for the targeted cells, and does not affect cell functions such as growth, differentiation and biological activity.[26]

For magnetic labelling, 10^6 cells per mL were incubated for 4 h in a sterilised suspension of nanoparticles dispersed in serum free RPMI supplemented with 5 mM sodium citrate at a final iron concentration of 1 mM. Incubation was followed by a 2 h chase at 37 °C in a nanoparticle free culture medium to ensure that all nanoparticles were internalised within the cells. Cells were then collected, centrifuged and resuspended at a cell concentration of 1×10^6 cells mL^{-1}. Magnetic labelling was performed with four different cell samples: (i) monocytes; (ii) macrophages; (iii) a mixture of monocytes and macrophages with a ratio of 90/10, and (iv) a mixture of monocytes and macrophages with a ratio of 50/50. Transmission Electron Microscopy was performed on a Zeiss EM902 instrument (platform MIMA2, INRA, Jouy-en-Josas, France).

Chip design and interfacing

The free-flow magnetophoresis chip design (Fig. 1A) featured an inlet channel for the cell suspension (100 μm wide), a branched inlet network for buffer solution, an 8 mm long and 3 mm wide separation chamber supported by ten square posts, as well as ten outlet channels (300 μm wide) merging into five separate outlets. The chip was fabricated in glass following conventional methods[46] and etched to a depth of 70 μm.

At the inlets, pipette tips acted as sample and buffer reservoirs. Each of the five outlets was connected to a 2 mL syringe *via* capillaries (i.d. 540 μm, o.d. 655 μm, Polymicro) and tubing (i.d. 640 μm, o.d. 900 μm, Saint-Gobain Performance Plastics). The syringes were mounted onto a syringe pump (PHD2000, Harvard Apparatus) operating under withdrawal mode at flow rates between 25 μL min^{-1} and 60 μL min^{-1}, corresponding to velocities of 2 mm s^{-1} to 4.8 mm s^{-1} in the separation chamber.

For observation, the chip was placed onto an inverted microscope, equipped with 1.6× and 4× objectives and a coolsnap HQ2 camera (Roper Scientific). For visualisation of cell trajectories, ten images, taken every 0.5 s, were overlaid.

To prevent cell adhesion, the channel walls were coated with serum albumin (PBS with 1% BSA, Sigma-Aldrich) for 30 min at 5 μL min^{-1}. For each sorting experiment, 500 μL of cell suspension with 1×10^6 cells mL^{-1} were introduced into the cell reservoir and 2 mL buffer into the buffer reservoir. Each sorting experiment was performed three times.

Cellular iron load quantification and magnetic set-up

Magnetic loading of cells was measured *via* a technique termed single-cell magnetophoresis.[45] Cells were placed into a cavity and subjected to a calibrated magnetic field gradient (gradB = 17 T m^{-1}, B = 145 mT). From video footage, the diameter (d_{cell}) and velocity of the cells towards the magnet ($\mathbf{v}_{cell}$) were measured. The magnetisation per cell (M_{cell}) and the iron nanoparticle load per cell could then be calculated. More specifically, by balancing the magnetic force ($\mathbf{F}_{mag} = M_{cell}\mathbf{grad}B$) with the viscous drag

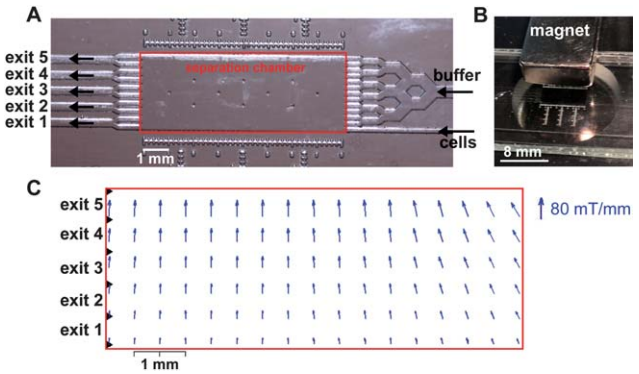

Fig. 1 (A) Photograph of the microfluidic chip showing the cell inlet, branched buffer inlet, the separation chamber supported by ten square posts and the five exit channels. (B) Photograph showing the positioning of the magnet on the top of the separation chamber. (C) Map of the magnetic field gradient inside the separation chamber calibrated by tracking the movement of beads of known magnetisation. GradB is represented by arrows with a spacing of 0.5 mm. The longest arrows correspond to a gradient of 80 mT mm^{-1}.

force ($\mathbf{F}_{vis} = 3\pi\eta d_{cell}\mathbf{v}_{cell}$), the magnetic moment M_{cell} of each single cell can be determined. It is more common to describe the magnetic loading of cells in terms of the equivalent mass of iron, m (pg), which is proportional to the cell magnetisation. For the maghemite nanoparticles used here, a magnetic moment of 6.6×10^{-14} A m^2 corresponds to 1 pg of iron. 200 cells were analysed per sample. These data could then also be used to calculate the expected trajectory of cells within the free-flow magnetophoresis chip.

The principle of continuous flow magnetic separation implies that magnetic objects are deflected from the sample flow stream by the application of a magnetic field perpendicular to the direction of flow. The magnetic field was generated by a NdFeB magnet (Calamit) that was 5 cm long, 1 cm wide and 4 mm thick. The magnet was positioned on the surface of the microchip with the help of reference points in the chip design (shown in Fig. 1B). The magnetic field at the magnet surface was 0.26 T, and in the middle of the separation chamber 0.15 T.

A map of the magnetic gradient **grad**B at different positions in the separation chamber was determined experimentally by tracking the velocities $\mathbf{v}_{bead}$ of magnetic beads (PMC-18, Kisker) of known diameter ($d_{bead} = 18$ μm) and known magnetic moment ($M_{bead} = 4.9 \times 10^{-12}$ A m^2) in the absence of flow, as detailed elsewhere.[37] Briefly, the magnetic force ($\mathbf{F}_{mag} = M_{bead}$ **grad**B) acting on the beads is balanced by the viscous drag force ($\mathbf{F}_{vis} = 3\pi\eta d_{bead}\mathbf{v}_{bead}$). Thus the local magnetic gradient equals

$$\mathbf{grad}\mathrm{B} = 3\pi\eta d_{bead}\mathbf{v}_{bead}/M_{bead}. \quad (1)$$

The separation chamber was divided into square sections of 500 μm side length. The velocities of 20 magnetic beads passing through each of these sections were averaged and the corresponding magnetic field gradient calculated. The obtained gradient map, shown in Fig. 1C, featured gradients ranging from 30 mT mm^{-1} to 80 mT mm^{-1}.

From the gradient map, the deflection path ($\mathbf{u}_{cell}$) of a cell with magnetic moment M_{cell} and diameter d_{cell} can be calculated based on summing the vector of the applied flow velocity $\mathbf{u}_{flow}$ in the flow direction and the vector of the magnetic velocity $\mathbf{u}_{mag}$ in the direction of the magnetic gradient:

$$\mathbf{u}_{cell} = \mathbf{u}_{flow} + \mathbf{u}_{mag} \quad (2)$$

with

$$\mathbf{u}_{mag} = M_{cell}\mathbf{grad}\mathrm{B}/3\pi\eta d_{cell} \quad (3)$$

Flow cytometry analysis

Quantitative fluorescence analysis was performed using a fluorescence-activated flow cytometer (Coulter xL4c). Before magnetic labelling, macrophages were labelled with the green fluorescent lipophilic membrane marker PKH-67 (Sigma-Aldrich). Monocytes and macrophages, before or after sorting, were characterised both by light scattering, to assess the relative size and granularity, as well as green fluorescence (excitation at 488 nm, emission at 525 nm). For each flow cytometric analysis, 10 000 events were recorded.

Results and discussion

Differential endocytosis of magnetic nanoparticles

To establish the extent of differential nanoparticle internalisation, monocytes and macrophages were labelled with magnetic nanoparticles by incubation with 1 mM extracellular iron for 4 h as outlined in the Experimental section. TEM images of the cells are displayed in Fig. 2A. These images show that for both monocytes and macrophages, small agglomerates of nanoparticles were distributed within intracellular compartments, *i.e.* the endosomes, as previously demonstrated for other cell types, including immune cells, malignant cells, muscle cells and stem cells.[26] Furthermore, it can clearly be seen that nanoparticles were captured much more efficiently by macrophages compared

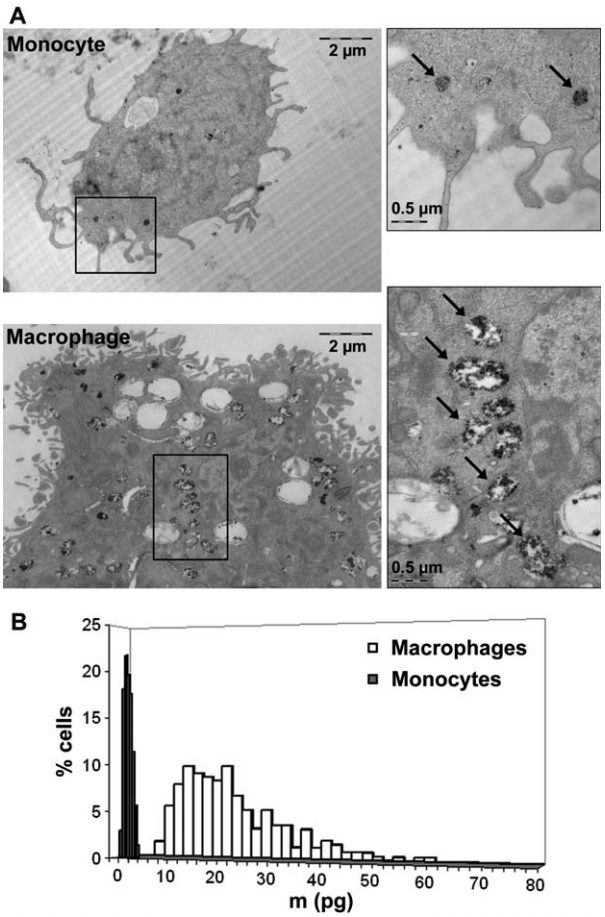

Fig. 2 (A) TEM images of monocytes (top) and macrophages (bottom) incubated with magnetic nanoparticles for 4 h at an extracellular iron concentration of 1 mM. Magnetic nanoparticles are dense to electrons and are therefore visible as black areas inside the cells. Nanoparticles were localised within intracellular compartments resembling endosomes. Magnified images of these magnetic endosomes are shown on the right hand side. Arrows indicate endosomes loaded with magnetic nanoparticles. It clearly appears that the magnetic endosomes were much more numerous, and more loaded with nanoparticles in the macrophages compared to the monocytes. (B) The distribution of iron load per cell, expressed in pg of iron, was measured for 200 individual cells by single cell magnetophoresis. Nanoparticles were taken up much less efficiently by the monocytes with a mean iron load of 2.2 pg per cell, compared to the macrophages which featured a mean iron load of 20 pg per cell.

to monocytes, for an incubation condition not previously tested, and in agreement with earlier studies.[43] The nanoparticle load was then quantified by single-cell magnetophoresis. The distributions of iron load over the monocyte and macrophage cell populations are illustrated in Fig. 2B. Macrophages were found to internalise ten times more nanoparticles than monocytes, with a mean iron load of 20 pg and 2.2 pg, respectively. This variation in internalisation of magnetic nanoparticles directly reflects specific cell functions, macrophages being in part targeted at endocytosing and phagocytosing cellular debris and pathogens.[47] The large distribution of iron load within each cell population must also be noted, with relative standard deviation more pronounced for macrophages (52%) than for monocytes (35%), reflecting different endocytotic capacities among the cell populations. When incubating other cell types with the anionic magnetic nanoparticles used here, the relative standard deviation was always found to range from 35% to 42%.[26] The high value obtained for macrophages reflects large discrepancies with regard to the internalisation capacities from one macrophage to another, probably due to the differentiation process from monocytes to macrophages, adding sources of heterogeneity in behaviour.

Having confirmed the differences in nanoparticle internalisation, the cells were studied within the microfluidic separation device.

Macrophage sorting according to magnetic loading

In a first series of experiments, macrophages were introduced into the free-flow magnetophoresis device in order to study the deflection and sorting of these cells based on their magnetic loading. As shown in Fig. 2B, the iron load per cell within the macrophage population ranged from 6 pg to 60 pg. Using the gradient map shown in Fig. 1C, it was possible to predict the trajectory of a cell in the separation chamber based on its magnetic loading, which corresponds to a given magnetic moment. The expected trajectories for cells with five different iron loads, namely 6, 15, 30, 45 and 60 pg per cell, were simulated for two withdrawal rates of 50 and 25 μL min^{-1}, corresponding to 4 mm s^{-1} and 2 mm s^{-1}. These are plotted in Fig. 3A. The deflection path and therefore the outlet taken by a cell are influenced by both the applied flow rate and the magnetic load (see eqn (2) and (3)). A slower flow rate and higher magnetic loading resulted in a larger extent of deflection and therefore a higher outlet number taken. Photographs from the corresponding experiments are displayed in Fig. 3B. It can be seen that the experimentally observed deflection paths corresponded very well to the simulated paths. Cells were found to leave the chamber through exits 1 to 4 for the 4 mm s^{-1} flow rate and through all five exits for the 2 mm s^{-1} rate, with some cells reaching the opposite wall of the chamber, and finally exiting through outlet 5.

A series of experiments was then performed at the 2 mm s^{-1} flow rate with collection of cells into outlet syringes and subsequent analysis. Examination of the number of cells collected at each outlet in relation to the injected cells (Fig. 3C) showed that most cells were collected into outlet 2. The total number of cells collected ranged from 85% to 92% of incoming cells. The magnetic loading of cell fractions collected at each outlet was then determined *via* single-cell magnetophoresis. The iron load distribution for each outlet cell sample, as well as the mean iron load at each outlet, are shown in Fig. 3D and E, respectively. The cellular magnetite loads at each exit were found to increase from low values to high values. An average of 10 pg iron per cell was found for cells exiting through outlet 1, whereas an average of 30 pg was found for cells exiting through outlet 5. The relative standard deviation for cellular iron load distributions at each outlet was in the range of 25–30%, much lower than the initial standard deviation of 53%. Taken together, these results demonstrate quantitatively that the extent of cell deflection increased with increasing iron load. It was thus possible to collect cells as a function of their magnetic properties. The cells collected are much more monodisperse in iron load than the injected population. As such magnetic properties are directly inferred by the cells' endocytotic capacities to internalise the 9 nm diameter magnetic nanoparticles, the cell subpopulations sorted into different outlet syringes correspond to cell populations with different endocytosis abilities.

Sorting of macrophage/monocyte mixtures

Considering the potential for sorting according to endocytotic cellular capacity, the next step was to apply the magnetic separation to two cell populations differing in their endocytosis function. An immediate demonstration of this application was therefore to attempt the purification of monocyte-derived macrophages from the original monocytes. Cell samples with monocyte/macrophage mixtures of 90/10 and 50/50 were injected into the microdevice. Fig. 4A shows an image from the sorting of the 90/10 mixture at a flow rate of 2 mm s^{-1}. It represents a superposition of ten frames taken every 0.5 s. From the photograph, the two cell populations can be distinguished visually by their difference in size: the monocytes feature a slightly smaller average diameter of 13.5 μm compared to the macrophages with 18.9 μm. The monocytes were only slightly deviated from the direction of laminar flow and were found to leave the separation chamber mainly through exit 1, in accordance with their lower iron content. In contrast, the macrophages, larger in size, representing 10% of the cell mixture, were deviated along the same paths as found for the pure macrophage samples in Fig. 3B. The photographs in Fig. 4B show 50/50 mixtures at three different flow rates, 25, 50 and 60 μL min^{-1}, corresponding to 2, 4 and 4.8 mm s^{-1}. Again, most of the monocytes left *via* outlet 1. The macrophages were deflected towards all exits due to their higher and more distributed magnetic loading. It can also be seen that at the faster flow rates the extent of deviation diminished. For this 50/50 mixture, the number of cells collected in each outlet syringe, expressed as a percentage of the total cells injected, is shown in Fig. 4C for the three flow rates. Between 89 and 95% of the cells injected were collected, with no clear dependence on the applied flow rate, indicating the robustness of the separation method.

Flow cytometry analysis of the cell sorted populations

Flow cytometric analysis was undertaken in order to further clarify the ratio of macrophages and monocytes collected at the different outlets. Initially samples with monocytes only and with

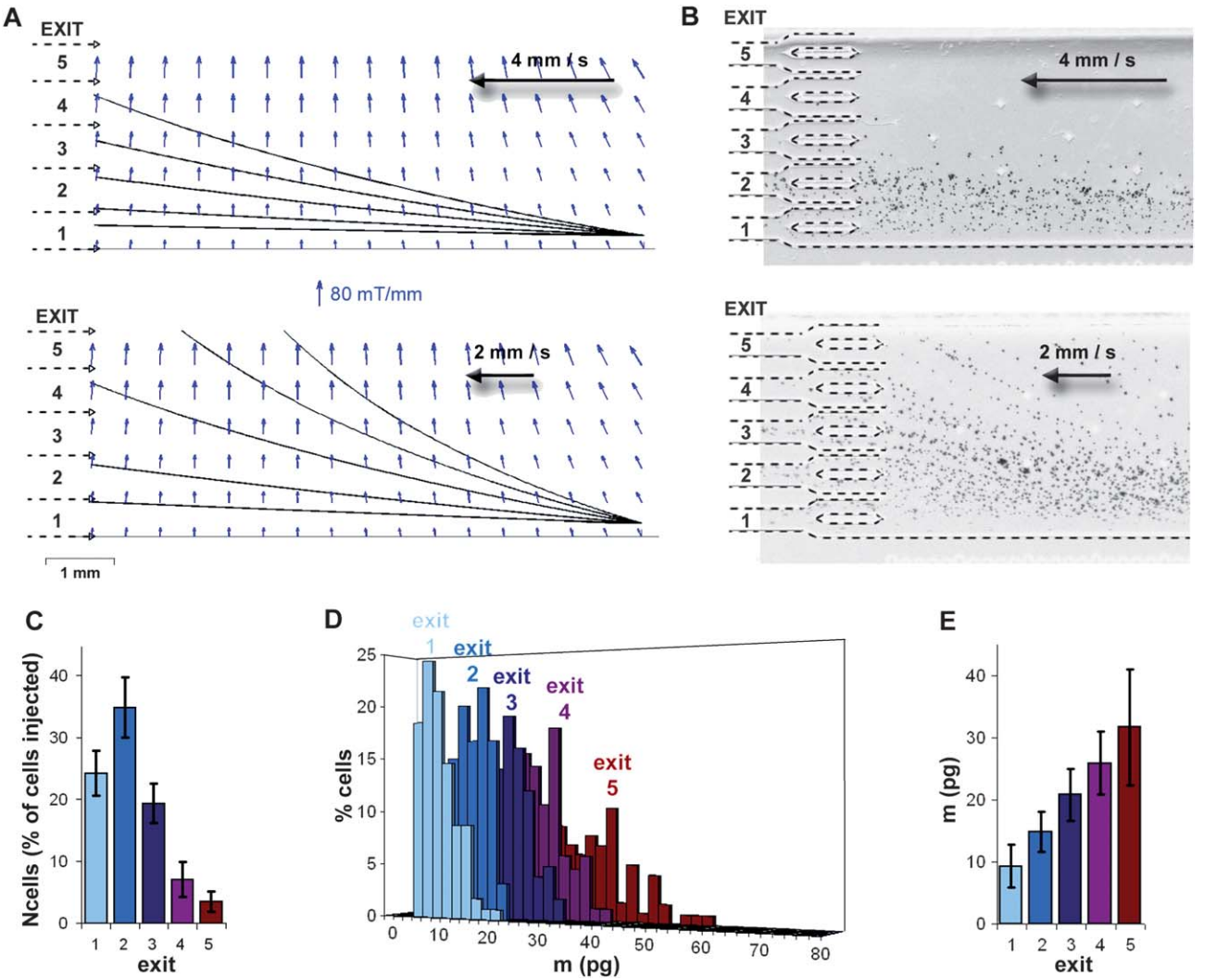

Fig. 3 (A) Calculated trajectories of 20 μm diameter spheres loaded with 6, 15, 30, 45 and 60 (from bottom to top) pg of iron were computed and superimposed on the map of the magnetic field gradient for two different flow velocities (top 4 mm s^{-1}, bottom 2 mm s^{-1}). (B) Experimental results from macrophage sorting performed for the two same flow conditions. The images represent the superposition of 10 frames that were recorded every 0.5 s, which makes it possible to visualise the cell tracks through the separation chamber. These were in good agreement with the calculated tracks as shown in (A), considering that the macrophages featured a mean diameter of 18.9 μm and iron loads ranging from 6 to 60 pg, with the most probable values between 10 and 20 pg. (C) Cells collected at each outlet for a flow rate of 2 mm s^{-1} were counted and are expressed as the % of the 500 000 cells injected into the chamber. (D) The cellular iron load of each cell fraction was quantified using single-cell magnetophoresis. (E) Finally, the mean iron load of the cell subpopulation collected at each outlet was determined. The higher the cellular iron load, the more pronounced was the deflection of cells, resulting in higher exit numbers of more highly loaded cells.

macrophages only were analysed on the flow cytometer. Monocytes exhibited a lower level of green fluorescence compared to the macrophages, while macrophages featured a larger side scattering signal due to their larger size and granulometry index. Therefore, monocytes were situated in the left, bottom quadrant of the fluorescence *versus* side scatter plot (Fig. 5A), whereas macrophages appeared in the right, top quadrant (Fig. 5B). Thus, both populations should be distinguished readily by flow cytometry analysis. Indeed, results for samples of initial monocyte/macrophage mixtures with 90/10 and 50/50 ratios are shown in Fig. 5C and D, respectively. The ratios obtained from the flow cytometric measurements were found to be 9.1 ± 0.5 for the 90/10 mixture, and 0.99 ± 0.02 for the 50/50 mixture, illustrating the robustness of the analysis.

Cell populations collected at outlets 1, 2 and 3 in sorting experiment of the 50/50 mixture at 2 mm s^{-1}, 4 mm s^{-1} and 4.8 mm s^{-1} were then analysed *via* flow cytometry and are displayed in Fig. 5E–G, H–J and K–M. Samples from outlets 4 and 5, as well as outlet 3 for the 4.8 mm s^{-1} flow rate, did not contain a sufficient number of cells and flow cytometry analysis was therefore not statistically significant. Monocytes were found to largely exit *via* outlets 1 and 2, whereas the outlets taken by the macrophages were highly dependent on the applied flow rate. At the faster flow rates, less deflection occurred so that for the fastest flow rate studied, the macrophages did not deflect much beyond outlet 2. Looking at the plots it becomes apparent that complete separation of the two cell populations could not be achieved, which would be expected based on the close iron loads shown in

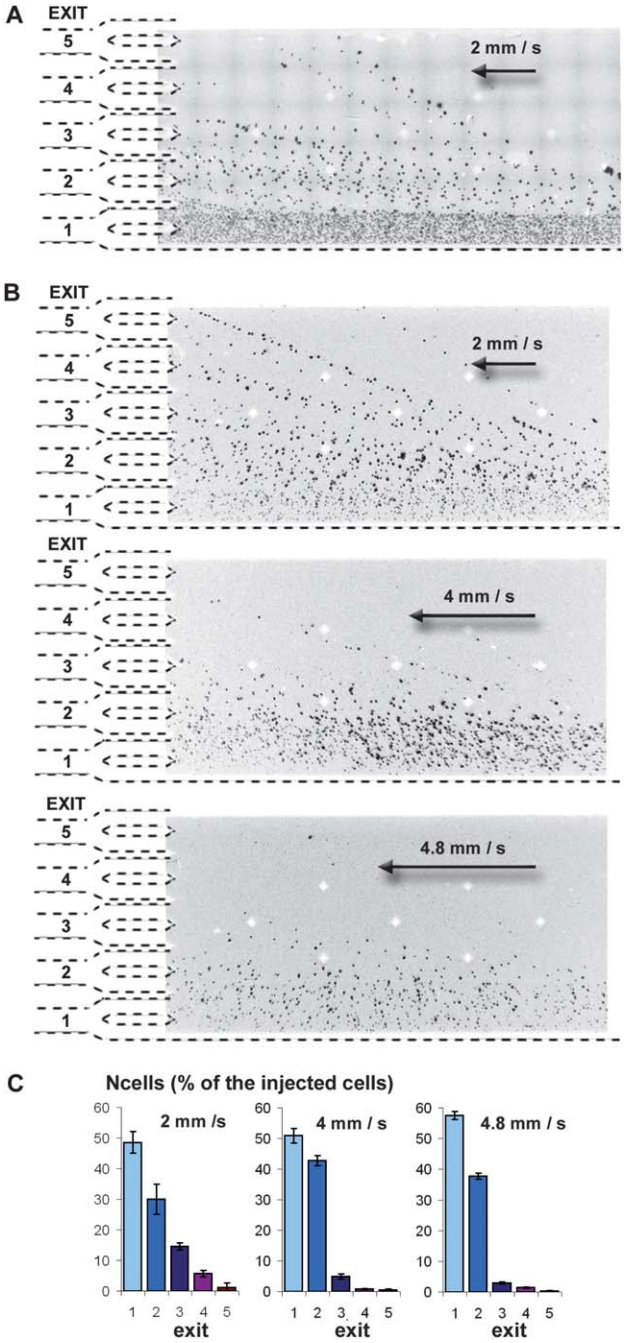

Fig. 4 (A) Tracks followed by monocytes and macrophages injected as a 90/10 mixture at 2 mm s^{-1}, obtained by superimposing 10 frames recorded every 0.5 s. Monocytes appear as smaller and less dark cells compared to the macrophages and are seen to exit mainly through outlet 1. (B) Monocyte and macrophapge trajectories for the 50/50 mixture at flow rates of 2 mm s^{-1}, 4 mm s^{-1} and 4.8 mm s^{-1}, obtained by superimposing 15 frames recorded every 0.4 s. It is still possible to visually distinguish monocytes from macrophages. Again, monocytes exit mainly though outlet 1; macrophages were found to deviate less when the flow rate was increased. (C) For the 50/50 mixture, the total number of cells collected at each outlet for the three flow rates was determined and is displayed as the percentage of the total number of injected cells, without distinction between macrophages and monocytes. The sum of the retrieved cells ranged from 89% to 95% of the injected cells.

Fig. 2B. However, by tuning the applied flow rate, the ratio of macrophages to monocytes in different outlets can certainly be tuned and significant enrichment can be achieved.

Quantitative data from flow cytometry experiments are collated into Fig. 6. In Fig. 6A, the relative proportion of macrophages and monocytes in the samples collected at the three exits is plotted for the 4 mm s^{-1} flow rate. In Fig. 6B the same data are presented for the 2 mm s^{-1} flow rate. By considering this ratio of monocytes to macrophages together with the total number of cells collected at each exit (see Fig. 4C), the number of one cell types collected at any one exit can be calculated and, in Fig. 6C and D, is expressed as the percentage of the total number of cells of this type injected. For both flow rates, the proportion of macrophages increases with the exit, exit 1 containing more monocytes and exits 2 and 3 more macrophages. The best enrichment of macrophages was obtained for the mixtures collected at exits 2 and 3 for the 2 mm s^{-1} flow rate. The cell mixture collected at exit 2 for this flow rate appears to be a good compromise for macrophage purification, when considering both the large number of cells (35% of the macrophages injected) with a desired enrichment (about 80% of macrophages in the mixture). It must be noted that the numbers of macrophages recolted from the 50/50 mixture at 2 mm s^{-1} (Fig. 6D, grey bars) are in perfect agreement with the ones from macrophages only (Fig. 3C). The role of the flow rate is exemplified in Fig. 6E and F, where the numbers of cells for each cell type are presented as a function of the three flow rates, for the two first exits 1 and 2. For both exits, the quicker the flow, the more macrophages end up in these low outlets. Finally, the condition of a 4.8 mm s^{-1} flow with cells recolted at exit 2 exhibit the best enrichment in macrophages (88% macrophages *versus* 12% monocytes) together with a significant number of cells (65% of the macrophages injected).

Significance and potential applications

To study cells individually, it is important to separate them from complex mixtures. Novel sorting methods combining low cost and finely tuned separation are highly desirable. Miniaturised cell separation devices offer fast and efficient separation with small sample volumes, and have the advantage of being easy to integrate with downstream analytical techniques. The development of microfluidic devices has therefore the potential for use in medical diagnostics.

Here, we have successfully tested magnetic cell separations in a novel microfluidic system which incorporated five outlets. We demonstrated that the cells were deflected and carried into the different outlet channels depending on their magnetic content. We could distinguish between cells with similar magnetic properties, corresponding to magnetic loadings between 10 and 30 pg (see Fig. 3D and E). Sorting of cells with such small variations in magnetite content has not previously been demonstrated. In contrast, a recent study showed sorting of cells labelled with antibody decorated magnetic beads for tagging based on molecular recognition. Different types of beads were used that varied in magnetisation by an order of magnitude to permit the sorting of cell types.[24] These cell separations therefore demonstrated that it was possible to sort, with excellent purity, different cell types using different magnetic tags. Here we prove that it is also possible to sort cells among a single cell population

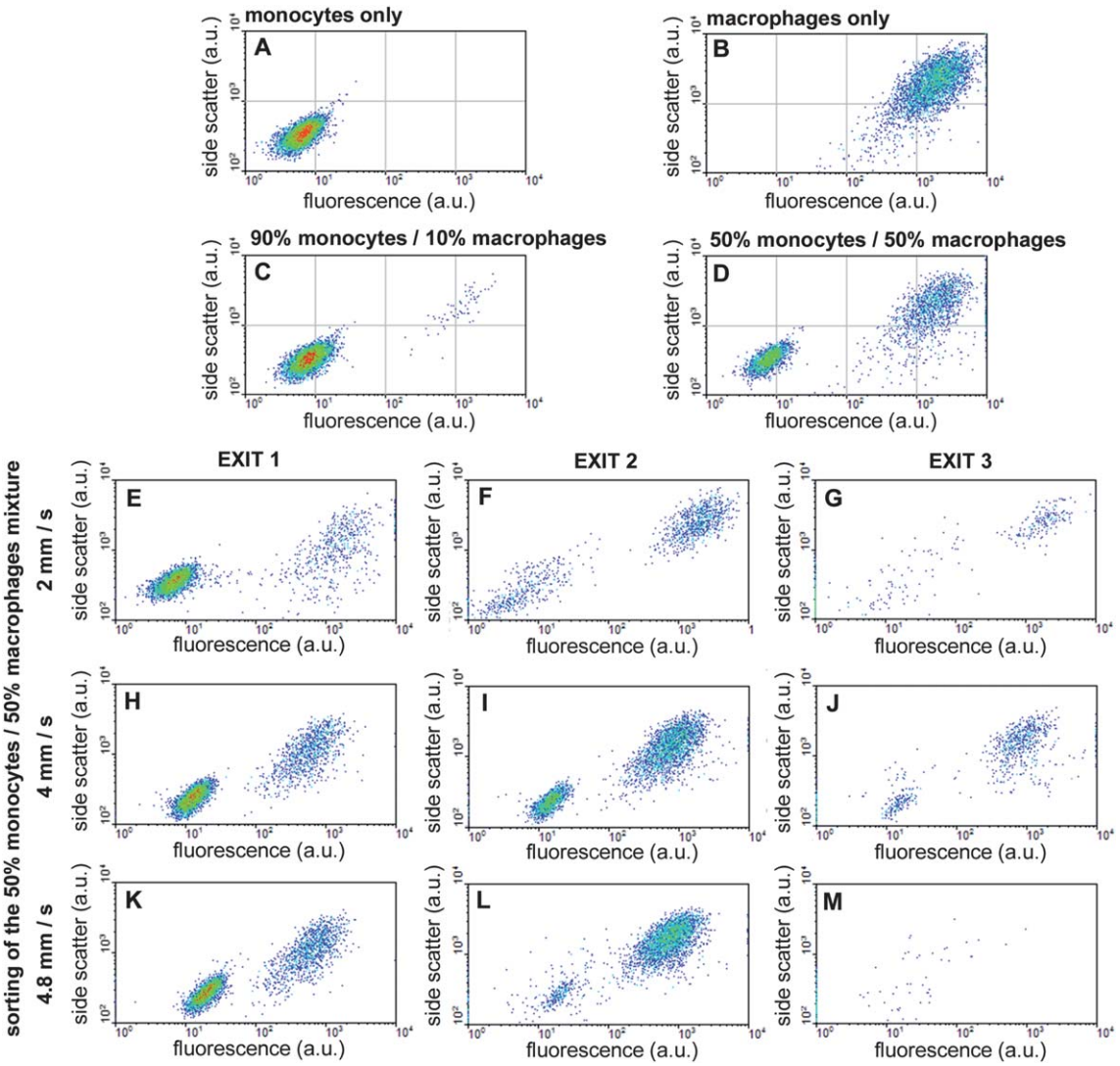

Fig. 5 Flow cytometry analysis of monocyte/macrophage mixtures before and after sorting. 10 000 events were recorded, representing between 6000 and 9000 cells depending on the degree of small impurities detected by the apparatus. For each cell, the intensity of green fluorescence and side scattering were measured. (A) Plot of a monocytes only sample. Monocytes alone showed a relatively low level for both the side scatter and the fluorescence signals and therefore appeared in the bottom left quadrant. (B) Plot of a macrophages only sample: macrophages exhibited relatively high fluorescence and side scattering signals and were therefore recorded in the top, right quadrant. (C) Plot of a 90/10 mixture of monocytes and macrophages. (D) Plot of a 50/50 mixture of monocytes and macrophages. The two cell populations can clearly be distinguished. (E–M) Flow cytometry data for samples collected at the three first exits during sorting experiments with 50/50 mixtures: exit 1 (E, H, K), exit 2 (F, I, L), exit 3 (G, J, M) for flow rates of 2 mm s^{-1} (E–G), 4 mm s^{-1} (H–J) and 4.8 mm s^{-1} (K–M).

according to the variation in their capacities to capture magnetic particles. The mechanism involved in this is the endocytosis of magnetic nanoparticles and the five cell populations collected (Fig. 3) correspond to cells with different endocytotic capacities, with direct application for biological studies of cell endocytosis. In addition, such separations could also be utilised for the selection of cells according to the expression of specific markers on the cell surface, with the appropriate antibody bound to the magnetic nanoparticles.

For a powerful separation system, it is then beneficial not only to separate cells of the same type with different magnetic contents, but also to separate different cell types. This was shown for the monocyte/macrophage system. Monocytes differentiate into macrophages at sites of inflammation and infection and the differentiated macrophages present an increase in endocytotic capacity. The magnetic tagging of a mixture of monocytes and macrophages was performed in a single step incubation. The separation of macrophages from monocytes showed a good purity (>88%), efficacy (>60%) and throughput (from 10 to 100 cells s^{-1}).

In addition to the immediate advantage of low cost compared to flow cytometry sorting, this microfluidic magnetic approach is probably also more efficient to discriminate cells with different endocytotic capacities. Indeed, if such sorting was envisaged using endocytotic fluorescent markers and flow cytometry, one should avoid specific markers targeting a given receptor and limit to a specific fluid phase endocytosis, with amounts of cellular internalized markers too low to allow an efficient sorting based on the fluorescence functionality.

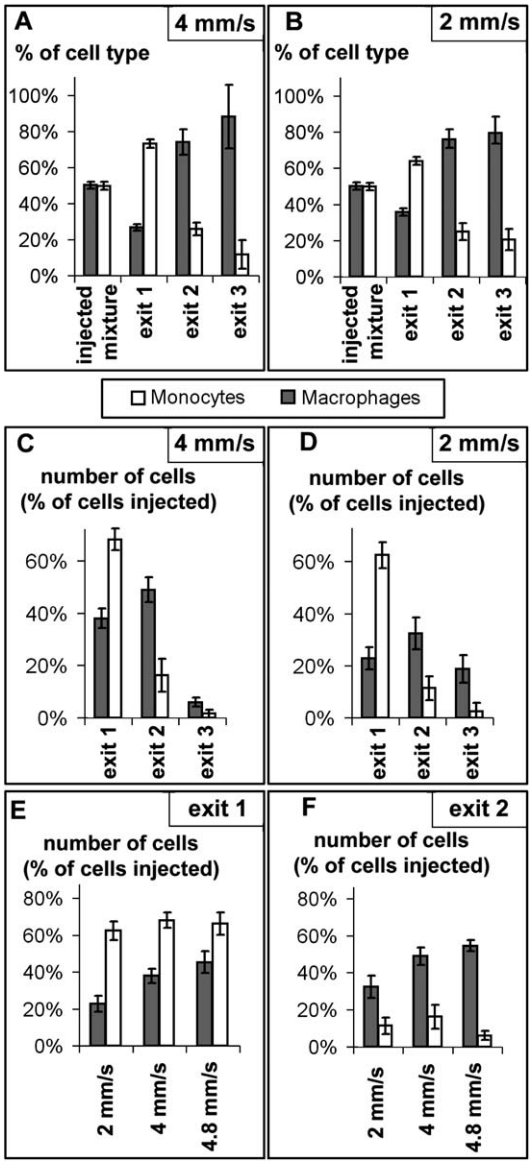

Fig. 6 (A) Fraction of monocytes *versus* macrophages in the initial injected mixture and in the mixtures collected at exits 1, 2 and 3 as calculated from the flow cytometric data for the flow speed of 4 mm s^{-1} (B) Fraction of monocytes *versus* macrophages at the flow speed of 2 mm s^{-1}. (C) The number of macrophages and monocytes collected at each outlet, expressed as the fraction of the cells injected for the corresponding cell type for the 4 mm s^{-1} flow rate. (D) The number of cells collected at each outlet expressed as the fraction of initially injected cells of the type for 2 mm s^{-1} flow rate. (E) The number of cells collected at exit 1 presented as a function of the three flow rates applied. (F) The number of cells collected at outlet 2 as a function of flow rate.

The proof of concept experiments on the sorting of macrophages based on their enhanced endocytotic capacities presented here opens new windows for diagnosis. Monocytes/macrophages play major roles as mediators of the immune response. However it is has become progressively established that the generic designation of macrophages hides highly dynamic and heterogeneous behaviours.[48] The functional properties of macrophages are constrained by several factors such as the heterogeneity of the precursor circulating monocytes,[49] their responsiveness to different stimuli (*i.e.* microbial products)[50] or the microenvironment of their homing tissue (lung alveolar space, adipose tissue, intestines, *etc.*).[51–53] In particular, the endocytosis/phagocytosis capacities of macrophages are strongly dependent on these dynamic phenotypes.[54] A method to separate macrophages with different uptake capacity is thus highly desirable. It could be used to isolate macrophages of different functional status or macrophages displaying different responses to microorganisms. Of particular interest is the versatility of macrophage polarisation. Depending on environmental cues, polarised macrophages can exert various and sometimes opposite functions, even when derived from the same precursor. Classical M1 polarisation features macrophages with antimicrobial and pro-inflammatory properties. However M1 macrophages can switch to the alternative M2 polarisation, demonstrating anti-inflammatory and regenerative properties.[55] Beyond infection, M2 macrophages can resolve inflammation through their high endocytotic clearance capacities.[56] We have recently observed that magnetic nanoparticles were taken up to different extents by macrophages with distinct polarisation (data not shown). Therefore selective magnetic sorting using the presented set-up could be valuable for isolating macrophages with different functions, including functions related to therapeutic regeneration.

More generally, it must be emphasised that the ability to obtain cell samples with identical magnetic properties is of particular interest for the rapidly developing medical fields of cell imaging and cell therapies with magnetic cells. Magnetic nanoparticles are clinically approved contrast agents for Magnetic Resonance Imaging (MRI). When incorporated into cells, they transfer their contrast properties to the cells themselves, becoming detectable on MRI scans. It has been demonstrated recently that single cells tagged *ex vivo* with magnetic nanoparticles and injected *in vivo* could be detected with MRI in living animals at their sites of migration.[57–59] Such an *in vivo* tracking of injected cells is of crucial importance for the evaluation of cell therapies with immune cells or stem cells. In addition, the ability of the magnetically labelled cells to be guided with external magnetic fields has also recently been investigated as a means to capture stem cells at sites of interest, *e.g.* in the heart, or as a means to retain stem cells in a cellular graft.[60,61] For these two types of applications a narrow distribution of the magnetic cellular content among the cell population used *in vivo* is desirable, and magnetically selective cell separation devices, such as the one presented here, are urgently needed.

Conclusions

A microfluidic device for magnetic cell separation as a function of cells endocytotic capacities has been designed, built and evaluated using a monocyte/macrophage model. The simple device comprised of a microfluidic flow cell and an external magnet. The device performance was in line with theoretical calculations. The requirement for small sample volumes and the excellent specificities and yield render this device as an asset for its integration into multi-step analysis microfluidic platforms. The sorting performed here concerns the purification of monocyte-derived macrophage from their respective native monocytes, with direct applications for further studies of macrophages biological functionalities. Furthermore, the precise selection of cells

within a small range of magnetic cellular content, as demonstrated here, opens new windows for the use of magnetic cells in cellular imaging or cell therapies.

Acknowledgements

We acknowledge Nathalie Luciani and Mark Tarn for fruitful discussions, Christine Ménager for providing us with the iron oxide magnetic nanoparticles and Christine Péchoux and Sophie Chat for electron microscopy observations. This work has been supported by the European project Magnifyco (Contract NMP4-SL-2009-228622).

Notes and references

1 A. K. Gupta and M. Gupta, *Biomaterials*, 2005, **26**, 3995–4021.
2 A. Ito, M. Shinkai, H. Honda and T. Kobayashi, *J. Biosci. Bioeng.*, 2005, **100**, 1–11.
3 J. L. Corchero and A. Villaverde, *Trends Biotechnol.*, 2009, **27**, 468–476.
4 Q. A. Pankhurst, N. K. T. Thanh, S. K. Jones and J. Dobson, *J. Phys. D: Appl. Phys.*, 2009, **42**, 224001.
5 M. Modo, M. Hoehn and J. W. Bulte, *Mol. Imaging*, 2005, **4**, 143–164.
6 E. S. Day, J. G. Morton and J. L. West, *J. Biomech. Eng.*, 2009, **131**, 074001.
7 M. Levy, C. Wilhelm, J. M. Siaugue, O. Horner, J.-C. Bacri and F. Gazeau, *J. Phys.: Condens. Matter*, 2008, **20**, 204133.
8 A. K. Gupta, R. R. Naregalkar, V. D. Vaidya and M. Gupta, *Nanomedicine (London, U. K.)*, 2007, **2**, 23–39.
9 B. Polyak and G. Friedman, *Expert Opin. Drug Delivery*, 2009, **6**, 53–70.
10 M. Babincova and P. Babinec, *Biomed. Pap. Med. Fac. Univ. Palacky Olomouc Czech Repub.*, 2009, **153**, 243–250.
11 F. Scherer, M. Anton, U. Schillinger, J. Henke, C. Bergemann, A. Kruger, B. Gansbacher and C. Plank, *Gene Ther.*, 2002, **9**, 102–109.
12 S. C. McBain, H. H. Yiu and J. Dobson, *Int. J. Nanomed.*, 2008, **3**, 169–180.
13 M. S. Martina, C. Wilhelm and S. Lesieur, *Biomaterials*, 2008, **29**, 4137–4145.
14 S. Marion, C. Wilhelm, H. Voigt, J. C. Bacri and N. Guillen, *J. Cell Sci.*, 2004, **117**, 3271–3279.
15 C. Wilhelm, *Phys. Rev. Lett.*, 2008, **101**, 028101.
16 L. J. Zhang and T. J. Webster, *Nano Today*, 2009, **4**, 66–80.
17 K. Ino, M. Okochi, N. Konishi, M. Nakatochi, R. Imai, M. Shikida, A. Ito and H. Honda, *Lab Chip*, 2008, **8**, 134–142.
18 A. Ito, K. Ino, M. Hayashida, T. Kobayashi, H. Matsunuma, H. Kagami, M. Ueda and H. Honda, *Tissue Eng.*, 2005, **11**, 1553–1561.
19 G. Frasca, F. Gazeau and C. Wilhelm, *Langmuir*, 2009, **25**, 2348–2354.
20 H. H. Yang, S. Q. Zhang, X. L. Chen, Z. X. Zhuang, J. G. Xu and X. R. Wang, *Anal. Chem.*, 2004, **76**, 1316–1321.
21 S. Miltenyi, W. Muller, W. Weichel and A. Radbruch, *Cytometry*, 1990, **11**, 231–238.
22 J. Dobson, *Nat. Nanotechnol.*, 2008, **3**, 139–143.
23 H. Lee, E. Sun, D. Ham and R. Weissleder, *Nat. Med.*, 2008, **14**, 869–874.
24 J. D. Adams, U. Kim and H. T. Soh, *Proc. Natl. Acad. Sci. U. S. A.*, 2008, **105**, 18165–18170.
25 V. Mailander, M. R. Lorenz, V. Holzapfel, A. Musyanovych, K. Fuchs, M. Wiesneth, P. Walther, K. Landfester and H. Schrezenmeier, *Mol. Imag. Biol.*, 2008, **10**, 138–146.
26 C. Wilhelm and F. Gazeau, *Biomaterials*, 2008, **29**, 3161–3174.
27 J. A. Frank, H. Zywicke, E. K. Jordan, J. Mitchell, B. K. Lewis, B. Miller, L. H. Bryant and J. W. Bulte, *Acad. Radiol.*, 2002, **9**, S484–S487.
28 T. T. Hansel, I. J. De Vries, T. Iff, S. Rihs, M. Wandzilak, S. Betz, K. Blaser and C. Walker, *J. Immunol. Methods*, 1991, **145**, 105–110.
29 I. Safarik and M. Safarikova, *J. Chromatogr., B: Biomed. Sci. Appl.*, 1999, **722**, 33–53.
30 G. D. Chen, C. J. Alberts, W. Rodriguez and M. Toner, *Anal. Chem.*, 2010, **82**, 723–728.
31 S. H. Song, H. L. Lee, Y. H. Min and H. I. Jung, *Sens. Actuators, B*, 2009, **141**, 210–216.
32 J. Kim, H. H. Lee, U. Steinfeld and H. Seidel, *IEEE Sens. J.*, 2009, **9**, 908–913.
33 C. Iliescu, G. Xu, E. Barbarini, M. Avram and A. Avram, *Microsyst. Technol.*, 2009, **15**, 1157–1162.
34 N. Pamme, *Lab Chip*, 2007, **7**, 1644–1659.
35 N. Pamme, *Lab Chip*, 2006, **6**, 24–38.
36 J. N. Krishnan, C. Kim, H. J. Park, J. Y. Kang, T. S. Kim and S. K. Kim, *Electrophoresis*, 2009, **30**, 1457–1463.
37 N. Pamme and C. Wilhelm, *Lab Chip*, 2006, **6**, 974–980.
38 Y. Jing, L. R. Moore, P. S. Williams, J. J. Chalmers, S. S. Farag, B. Bolwell and M. Zborowski, *Biotechnol. Bioeng.*, 2007, **96**, 1139–1154.
39 T. Schneider, S. Karl, L. R. Moore, J. J. Chalmers, P. S. Williams and M. Zborowski, *Analyst*, 2010, **135**, 62–70.
40 N. Beckmann, C. Cannet, A. L. Babin, F. X. Ble, S. Zurbruegg, R. Kneuer and V. Dousset, *Wiley Interdiscip. Rev.: Nanomed. Nanobiotechnol.*, 2009, **1**, 272–298.
41 A. Beduneau, Z. Ma, C. B. Grotepas, A. Kabanov, B. E. Rabinow, N. Gong, R. L. Mosley, H. Dou, M. D. Boska and H. E. Gendelman, *PLoS One*, 2009, **4**, e4343.
42 M. R. Choi, K. J. Stanton-Maxey, J. K. Stanley, C. S. Levin, R. Bardhan, D. Akin, S. Badve, J. Sturgis, J. P. Robinson, R. Bashir, N. J. Halas and S. E. Clare, *Nano Lett.*, 2007, **7**, 3759–3765.
43 N. Luciani, F. Gazeau and C. Wilhelm, *J. Mater. Chem.*, 2009, **19**, 6373–6380.
44 R. Massart, *IEEE Trans. Magn.*, 1981, **17**, 1247–1248.
45 C. Wilhelm, F. Gazeau and J. C. Bacri, *Eur. Biophys. J.*, 2002, **31**, 118–125.
46 T. McCreedy, *TrAC, Trends Anal. Chem.*, 2000, **19**, 396–401.
47 J. D. Ernst and O. Stendahl, *Phagocytosis of Bacteria and Bacterial Pathogenicity*, Cambridge University Press, New York, 2006.
48 A. J. Rees, *Semin. Nephrol.*, 2010, **30**, 216–233.
49 S. Yona and S. Jung, *Curr. Opin. Hematol.*, 2010, **17**, 53–59.
50 M. Benoit, B. Desnues and J. L. Mege, *J. Immunol.*, 2008, **181**, 3733–3739.
51 J. M. Olefsky and C. K. Glass, *Annu. Rev. Physiol.*, 2010, **72**, 219–246.
52 D. L. Laskin, V. R. Sunil, C. R. Gardner and J. D. Laskin, *Annu. Rev. Pharmacol. Toxicol.*, 2011, **51**, 267–288.
53 A. Sica, P. Larghi, A. Mancino, L. Rubino, C. Porta, M. G. Totaro, M. Rimoldi, S. K. Biswas, P. Allavena and A. Mantovani, *Semin. Cancer Biol.*, 2008, **18**, 349–355.
54 M. Leidi, E. Gotti, L. Bologna, E. Miranda, M. Rimoldi, A. Sica, M. Roncalli, G. A. Palumbo, M. Introna and J. Golay, *J. Immunol.*, 2009, **182**, 4415–4422.
55 A. Mantovani, C. Garlanda and M. Locati, *Arterioscler., Thromb., Vasc. Biol.*, 2009, **29**, 1419–1423.
56 F. O. Martinez, A. Sica, A. Mantovani and M. Locati, *Front. Biosci.*, 2008, **13**, 453–461.
57 W. Liu and J. A. Frank, *Eur. J. Radiol.*, 2009, **70**, 258–264.
58 A. S. Arbab and J. A. Frank, *Regener. Med.*, 2008, **3**, 199–215.
59 P. Smirnov, M. Poirier-Quinot, C. Wilhelm, E. Lavergne, J. C. Ginefri, B. Combadiere, O. Clement, L. Darrasse and F. Gazeau, *Magn. Reson. Med.*, 2008, **60**, 1292–1297.
60 B. Polyak, I. Fishbein, M. Chorny, I. Alferiev, D. Williams, B. Yellen, G. Friedman and R. J. Levy, *Proc. Natl. Acad. Sci. U. S. A.*, 2008, **105**, 698–703.
61 K. Cheng, T. S. Li, K. Malliaras, D. R. Davis, Y. Zhang and E. Marban, *Circ. Res.*, 2010, **106**, 1570–1581.

